Theoretical Study of Oxygen Isotope Exchange and Quenching in the O(^{1}D) + CO$_2$ Reaction[†]

A. M. Mebel,*[‡,§] M. Hayashi,[∥] V. V. Kislov,[§] and S. H. Lin*[,§]

Department of Chemistry and Biochemistry, Florida International University, Miami, Florida 33199, Institute of Atomic and Molecular Sciences, Academia Sinica, P.O. Box 23-166, Taipei 10764, Taiwan, and Center for Condensed Matter Sciences, National Taiwan University, #1 Roosevelt Rd. Sec. 4, Taipei 106, Taiwan

Received: February 15, 2004; In Final Form: March 31, 2004

Ab initio multireference configuration interaction calculations have been carried out for the CO$_3$ system in singlet and triplet electronic states to investigate the mechanism of the O(^{1}D) + CO$_2$ reaction. The reaction has been shown to occur through the formation of an O–CO$_2$ complex **s0**, which then isomerizes to a cyclic O=(CO$_2$) structure **s1** over a barrier at s-TS0 located ~0.3 kcal/mol below the reactants. The cyclic isomer **s1**, 48.8 kcal/mol lower in energy than O(^{1}D) + CO$_2$, can in turn rearrange to a D_{3h} structure **s2**, only slightly higher in energy. The isomers **s1** and **s2** formed in the reaction possess high internal energy and can decompose into the initial reactants or undergo singlet–triplet intersystem crossing to form the triplet isomer **t1**, which can dissociate to O(^{3}P) + CO$_2$. If the attacking oxygen atom is isotope-labeled, isotope exchange can occur due to symmetry properties of **s1** and **s2**. The ab initio energies, molecular parameters, and spin–orbit coupling constants were employed in statistical calculations of various isomerization and dissociation reaction rates. For intersystem crossing rates, we used the theory of radiationless transitions, in which the rates are determined as a product of the overlap of electronic wave functions (spin–orbit coupling) and the overlap of vibrational wave functions (Franck–Condon factor). The calculated rate constants were then used to compute the product branching ratios both for the case of the ^{16}O(^{1}D) + ^{44}CO$_2$ reaction and for the isotope-labeled ^{18}O(^{1}D) + ^{44}CO$_2$ reaction. For the latter, the calculated relative branching ratios of the ^{16}O(^{1}D) + ^{46}CO$_2$ and ^{16}O(^{3}P) + ^{46}CO$_2$ products at collision energies of 4.2 and 7.7 kcal/mol, 17/83 and 42/58, agree reasonably well with the experimental values of 16/84 and 33/67 (ref 4), respectively, and reproduce the qualitative trend with E_{col}. The overall relative yields computed for ^{44}CO$_2$ and ^{46}CO$_2$ show that the attacking O(^{1}D) atom can be incorporated into the product CO$_2$ molecule with a near-statistical probability of $^2/_3$.

Introduction

The quenching of O(^{1}D) by carbon dioxide, O(^{1}D) + CO$_2$, is relevant to the atmospheres of Earth and Mars. On Earth, photolysis of stratospheric ozone generates O(^{1}D), which in turn can collide with CO$_2$ to form a carbon trioxide molecule.[1,2] In the gas phase, the latter can fragment to carbon dioxide and atomic oxygen in the ground ^{3}P or excited ^{1}D electronic states.[3,4] Thus, the O(^{1}D) + CO$_2$ reaction can proceed either by an oxygen atom exchange mechanism, in which the products and reactants are equivalent, or by quenching of O(^{1}D) to O(^{3}P). The reaction is thought to be the source of[1,2] the observed enrichment of stratospheric CO$_2$ in the heavy isotopes ^{17}O and ^{18}O relative to tropospheric CO$_2$.[5–11] Stratospheric ozone is also enriched[10–14] in ^{17}O and ^{18}O, and, for the case of CO$_2$, it was suggested[1,2] that the anomalous oxygen isotopic composition of O$_3$ could be transferred to carbon dioxide by photolysis of O$_3$ to form O(^{1}D) followed by a quenching collision of the latter with CO$_2$, which can be accompanied by isotope exchange. The isotope labeling results of Baulch and Breckenridge[15] showed a near-statistical rate of isotope exchange for which the incoming O(^{1}D) atom has an approximately $^2/_3$ chance of being incorporated into the product CO$_2$ molecule, although the formation of O$_3$ in their system and their assumption that quenching occurs

at all collisions may have influenced this result. If, however, the isotope exchange mechanisms can be understood in detail, observation of the anomalous isotopic composition of CO$_2$ may provide a unique tracer of stratospheric chemistry and mass transport on annual time scales and a means to quantify gross carbon fluxes to and from the biosphere.[11,16,17] In the Martian atmosphere, carbon dioxide is the major constituent[18] (95.3 vol %), and its photodissociation by solar photons (λ < 2050 Å) produces CO and atomic oxygen in the ground ^{3}P state near threshold, but shorter wavelengths also supply O(^{1}D).[19] The primary fate of electronically excited oxygen atoms is thought to be quenching to the ^{3}P state; the detailed process is not known and has been postulated to proceed via a carbon trioxide molecule.[19–22]

The kinetics of the quenching of O(^{1}D) by CO$_2$ has received considerable attention,[23–25] and the reaction has been shown to proceed at a nearly gas kinetic rate of 1.1×10^{-10} cm^3 s^{-1} molecule^{-1}.[25] This order of magnitude suggests that the reaction has no or only little activation energy, proceeds with almost unit efficiency, and most likely involves a reaction intermediate. However, neither reaction products nor the nature of the intermediate were determined in the kinetic studies. For the first time, recent crossed molecular beam experiments[3,4] showed that the O(^{1}D) + CO$_2$ reaction can produce not only O(^{3}P) + CO$_2$ but also O(^{1}D) + CO$_2$ and provided the O(^{1}D)/O(^{3}P) branching ratios at several collision energies. As the measurements were carried out for the isotope-labeled ^{18}O(^{1}D) + ^{44}CO$_2$ reaction, they represented the first experimental evidence that the isotope

exchange can occur through a long-lived CO_3 intermediate without crossing to the triplet surface.[3,4]

Although some calculations of the CO_3 potential energy surface (PES) related to the $O(^1D) + CO_2$ reaction have been reported in the literature,[26] available theoretical data are not sufficient for quantitative prediction of the isotope exchange nonquenching/quenching branching ratio as a function of available energy. First, due to the fact that the wave function of $O(^1D)$ has a strong multireference character, to provide accurate energies, the calculations of the CO_3 PES, especially of its part related to the entrance channel of the $O(^1D) + CO_2$ reaction, must be performed using multireference methods of ab initio theory. Therefore, in the present work, we report the CO_3 PESs calculated using the highly accurate multireference configuration interaction (MRCI) method with large and flexible basis sets.

Second, even when an accurate PES for the CO_3 system is available, standard RRKM calculations of reaction rate constants are not sufficient to predict the product branching ratios because the quenching reaction channel leading to $O(^3P)$ involves a change in electronic multiplicity. Therefore, in addition to rate constants for conventional isomerization and dissociation reaction steps, we must consider reaction rates for intersystem crossing (ISC) processes. Several approaches exist to address this problem, including nonadiabatic dynamical studies or nonadiabatic statistical rate theories.[27-35] However, these approaches tend to significantly underestimate rate constants for the reactions with a multiplicity change. In the present work, we employ both nonadiabatic transition state theory and the theory of radiationless transitions[36-44] to compute the ISC rate constants and demonstrate that the latter approach is critical to reproducing the experimental results. The ISC rate constants are then combined with the rates obtained using RRKM theory and are used to predict the relative yields of the $O(^1D) + CO_2$ and $O(^3P) + CO_2$ products at various collision energies. Such calculations are performed for both the ^{16}O and the ^{18}O isotopes of $O(^1D)$, and comparisons are made with the experimental branching ratios reported by Perri et al.[4]

Methods of Ab Initio Calculations

Geometries of various intermediates and transition states on the singlet and triplet PESs of CO_3 have been optimized using the multireference complete active space self-consistent field (CASSCF) method[46] with the 6-311G(d) basis set. The active space in CASSCF calculations consisted of 16 electrons distributed on 13 orbitals, (16,13). These include all valence orbitals except three occupied orbitals corresponding to the 2s lone pairs of oxygen atoms. For the key intermediates **s1** and **s2**, we have also performed geometry optimization at the full-valence-active-space CASSCF(22,16)/6-311G(d) level. The optimized geometric parameters appeared to be very close to those obtained with the smaller (16,13) active space. Calculations of vibrational frequencies with the full-valence (22,16) active space were beyond our computational facilities. Hence, only CASSCF(16,13) calculations were performed for other species, assuming that a relative contribution of the 2s orbitals of O atoms into electronic correlation is not significant. Vibrational frequencies of various structures have been computed at the CASSCF(16,13)/6-311G(d) level of theory. For comparison, we have also carried out hybrid density functional B3LYP/6-311G(d)[46] geometry optimization and calculations of vibrational frequencies.

Energies of various structures were then refined by single-point calculations at the CASSCF(16,13)/6-311G(d) optimized geometries using higher levels of theory. For instance, we employed the internally contracted multireference configuration (MRCI) method[47] with larger 6-311+G(3df) and Dunning's correlation-consistent pvtz[48] basis sets. MRCI calculations were performed with the (16,13) active space, that is, the full-valence active space excluding 2s lone pairs of oxygens. However, initial wave functions for the MRCI calculations were obtained at the full-valence-active-space CASSCF(22,16) level. We have also included Davidson corrections for quadruple excitations into MRCI energies (MRCI+Q). In addition, for various intermediates and transition states on the lowest in energy triplet and singlet PESs, we carried out coupled cluster[49] CCSD(T) single-point energy calculations with the 6-311+G(3df) basis set.

The ab initio calculations described in this paper were performed using the DALTON,[50] MOLPRO 2002,[51] and Gaussian 98[52] program packages.

Potential Energy Surfaces of CO_3

In this study, we consider two singlet PESs correlated to the $O(^1D) + CO_2$ asymptote. The ^1D electronic state of the oxygen atom is five-fold degenerate, so when $O(^1D)$ and CO_2 approach each other from infinity, the asymptote splits into five PESs. However, only two of them are attractive at long separations; the other three exhibit a repulsive character and will not be considered thereafter, as they are not expected to play a role in the reaction, at least at low and moderate collision energies (below $10-15$ kcal/mol). The two surfaces included into our study are $^1A_1$ and $^1A_2$ within C_{2v} symmetry or $^1A'$ and $^1A''$ if the symmetry is lowered to C_s. Similar to the previous study,[26] we have found two deep local minima on the lowest singlet PES. One of them has a cyclic structure with a CO_2 ring and the third O atom connected with the central carbon by a double C=O bond (see Figure 1). The isomer **s1** (C_{2v}, $^1A_1$) resides 47.2 kcal/mol below $O(^1D) + CO_2$ at the MRCI+Q(16,13)/6-311+G-(3df) level (Figure 1 and Table 1). The second isomer **s2** has a D_{3h}-symmetric geometry, $^1A_1$ electronic state, and lies only 0.1 kcal/mol higher in energy than **s1**. As seen in Table 1, at different theoretical levels, the energy gap between **s2** and **s1** varies from 0.1 kcal/mol at MRCI+Q(16,13)/6-311+G(3df) to 1.1 and 3.3 kcal/mol at MRCI+Q(16,13)/pvtz and CCSD(T)/6-311+G(3df), respectively.

Let us consider now how **s1** and **s2** can be produced from the $O(^1D) + CO_2$ reactants. A transition state search for the approach of $O(^1D)$ toward carbon dioxide showed that, along the minimum energy reaction path (MEP), the attacking oxygen atom draws near both the central carbon and one of the terminal oxygens. We have studied the MEP at the CASSCF/6-311G(d) level by scanning the PES at fixed values of the O−C distance corresponding to the newly formed O−C bond, which were varied from 3.0 to 1.3 Å with a 0.1 Å step, allowing other geometric parameters to be optimized. According to the results of this scan, the MEP connects the reactants with the cyclic **s1** intermediate. Saddle-point optimization at this level of theory gave a structure where the O−C distance is about 2.07 Å and the O−O distance for the forming O−O bond is 1.72 Å. The reaction barrier obtained at CASSCF/6-311G(d) with ZPE corrections is 5.4 kcal/mol with respect to the initial reactants. However, recalculation of the single-point energy for this CASSCF-optimized transition state at the MRCI+Q/6-311+G(3df) level significantly decreases its relative energy, to −4.8 kcal/mol. Because dynamic correlation seems to be important for the transition state geometry and energy, geometry optimization of its structure has to be redone at a level of theory higher than CASSCF. As analytical gradients are not available for the MRCI method, we carried out single-point energy

Theoretical Study of the O(^{1}D) + CO$_2$ Reaction

J. Phys. Chem. A, Vol. 108, No. 39, 2004 **7985**
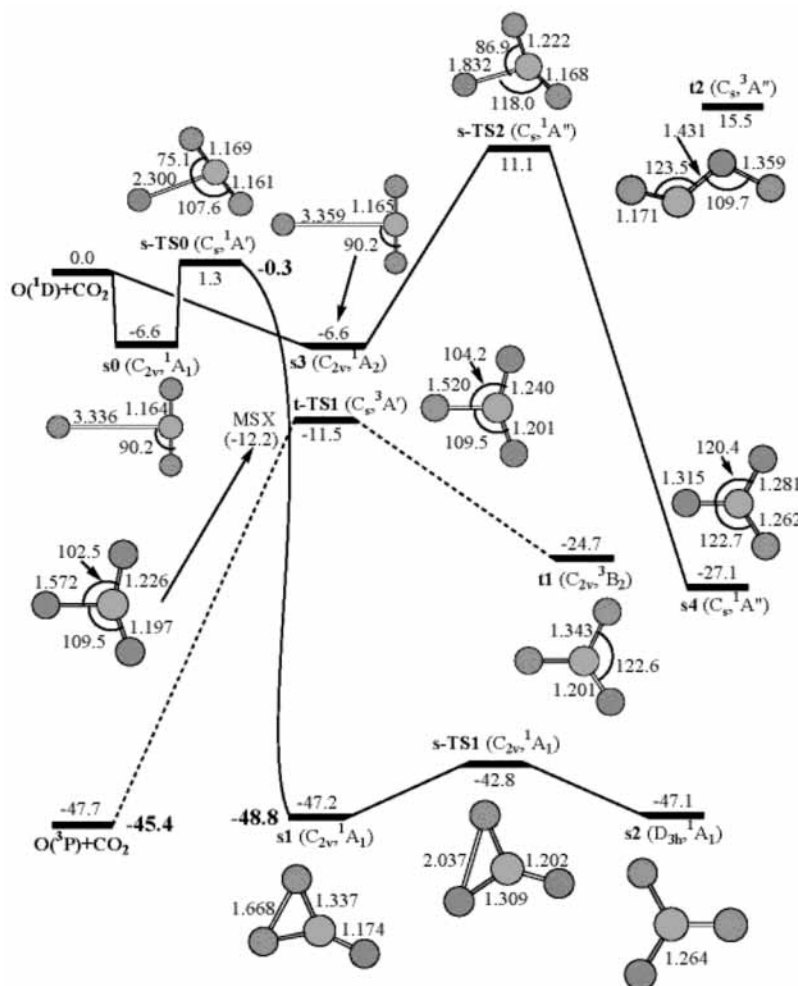
Figure 1. Potential energy diagram of the O(^{1}D) + CO$_2$ reaction calculated at the MRCI+Q(16,13)/6-311+G(3df)//CASSCF(16,13)/6-311G(d) + ZPE[CASSCF(16,13)/6-311G(d)] level of theory. All energies are given in kcal/mol. Bold numbers give best estimates for the relative energies of O(^{3}P) + CO$_2$, intermediate **s1**, and transition state s-TS0 (see text for detail). Geometric structures of various intermediates and transition states are also shown with bond lengths given in angstroms and bond angles given in degrees.

TABLE 1: Relative Energies (E_{rel}, kcal/mol) and Zero-Point Energies (ZPE, kcal/mol) of the Reactants, Products, Intermediates, and Transition States on the Singlet and Triplet Potential Energy Surfaces of the O(^{1}D) + CO$_2$ ⇆ CO$_3$ → O(^{3}P) + CO$_2$ Reactions Calculated at Various Levels of Theory

method	B3LY P/6-311 G(d)		CASSC F/6-311G (d)		MRCI/6-311+ G(3df)	MRCI +Q/6-311 +G(3df)	CCS D(T) /6-31 1+G(3df)	CASS CF/ pvtz	MR CI/ pvtz	MRCI+Q/ pvtz
species	ZPE	E_{rel}	ZPE	E_{rel}	E_{rel}	E_{rel}	E_{rel}	E_{rel}	E_{rel}	E_{rel}
O(^{1}D) + CO$_2$	7.35	0.00	7.35	0.00	0.00	0.00	0.00	0.00	0.00	0.00
s0			7.44	−1.84	−6.24	−6.59	−0.88	−0.60	−0.60	−0.64
s-TS0			7.62	5.44	2.27[a]	1.33[a]	−0.15[a]	8.09	2.69[a]	1.82[a]
s1	8.69	−13.52	8.54	−30.19	−44.97	−47.18	−51.41	−30.26	−45.15	−47.35
s-TS1	7.68	−2.68	7.36	−24.11	−40.10	−42.76	−47.10	−23.69	−39.56	−42.12
s2	7.99	−3.32	7.37	−25.62	−43.88	−47.08	−48.12	−25.16	−43.23	−46.29
s3	7.47	−1.08	7.43	−1.85	−6.24	−6.59		−1.88	−6.75	−7.17
s-TS2	7.16	12.17	6.87	27.61	14.15	11.06		27.55	14.18	11.26
s4	6.40	−2.80	6.07	−6.12	−24.02	−27.14		−6.27	−23.89	−26.92
O(^{3}P) + CO$_2$	7.35	−16.71	7.35	−50.45	−47.90	−47.67	−51.01	−50.55	−48.00	−47.75
t-TS1	6.60	2.30	5.90	3.23		−11.45[b]	−15.73			
t1	6.89	−7.90	7.69	−8.10	−22.26	−24.72	−29.00	−7.87	−22.07	−24.49
t2			7.03	32.63		15.54[b]	11.26			

[a] The barrier height is obtained using the search of the maximal point along the MEP energy profile calculated at the level of theory given in the column caption with geometries of MEP structures optimized at CASSCF/6-311G(d) (see text for detail). [b] For t-TS1 and **t2**, which have a low C_s symmetry, MRCI(16,13) calculations were beyond our computing facilities. The relative energies shown in the table are computed on the basis of the relative energy of **t1** at the MRCI+Q/6-311+G(3df) level (−24.72 kcal/mol) and the energies of t-TS1 and **t2** with respect to **t1** obtained at the CCSD(T)/6-311+G(3df) level (13.27 and 40.26 kcal/mol, respectively).

calculations along the CASSCF-optimized MEP at the MRCI+Q/ 6-311+G(3df), MRCI+Q/pvtz, and (additionally) CCSD(T)/6-311+G(3df) levels of theory and located the transition state as the maximal energy point along the MEP. At the MRCI+Q

level with both basis sets, the transition state s-TS0 is found at the O−C distance of ∼2.3 Å (see the optimized structure in Figure 1); at the CCSD(T)/6-311+G(3df) level, the transition state structure is looser and has an O−C distance of ∼2.6 Å.

The barrier for the $O(^1D) + CO_2 \rightarrow CO_3$ reaction is computed as 1.3 and 1.8 kcal/mol at the MRCI+Q/6-311+(3df) and MRCI+Q/pvtz levels, respectively, and at the CCSD(T) level the transition state resides 0.2 kcal/mol below the reactants. On the other hand, the barrier for the decomposition of **s1** to $O(^1D) + CO_2$ is computed as 48.5, 49.2, and 51.3 kcal/mol at the three levels of theory mentioned above, respectively − the dependence of the reaction rate constant on the barrier height will be seen in subsequent sections.

Transition state s-TS0 is not connected directly to the $O(^1D) + CO_2$ reactants, as the PES has an attractive character at long separations. CASSCF optimization gave a C_{2v}-symmetric $O\cdots CO_2$ complex on the $^1A_1$ surface designated as **s0** in Figure 1 with an O−C separation of 3.34 Å. The complex formation energy for **s0** appeared to be sensitive to the level of theory employed; it varies from 0.6 kcal/mol at MRCI+Q/pvtz to 0.9 and 1.8 kcal/mol at the CCSD(T) and CASSCF levels, respectively, but increases to 6.6 kcal/mol at MRCI+Q/6-311+G(3df). The formation of the most stable CO_3 isomer **s1** from the initial reactants is described by the following mechanism: $O(^1D) + CO_2 \rightarrow$ **s0** → s-TS0 → **s1**. The latter can further isomerize into the D_{3h}-symmetric **s2** structure, overcoming a relatively low barrier of 4.4 kcal/mol at a C_{2v}-symmetric transition state s-TS1. In turn, **s2** can rearrange back to **s1**, overcoming a slightly lower 4.3 kcal/mol barrier. Although the reversible **s1** ⇌ **s2** isomerization does not change the composition of **s1** when all oxygen atoms are identical, it becomes significant for isotope scrambling when one of the O's is isotope-labeled. All of the oxygen atoms are equivalent in the D_{3h} **s2** isomer so that the position of the isotope label can change after the **s1** ⇌ **s2** isomerization. It should be also noted that, according to the calculated MEP, structure **s2** cannot dissociate directly to the $O(^1D) + CO_2$ products; it must first rearrange to **s1** via the process **s2** → s-TS1 → **s1** → s-TS0 → **s0** → $O(^1D) + CO_2$, so that isotope exchange can occur even without IVR if **s2** is sampled.

On the $^1A_2$ PES, $O(^1D)$ and CO_2 form without a barrier a strongly bound complex **s3**, which has approximately the same geometry as **s0** and lies 6.6 and 7.2 kcal/mol lower in energy than the reactants at the MRCI+Q level with the 6-311+G-(3df) and pvtz basis sets, respectively. **s3** can rearrange into the CO_3 molecule in the excited electronic state $^1A''$, structure **s4**. The latter has a geometry similar to that of the D_{3h}-symmetric isomer **s2**, but all three C−O bond lengths are slightly different, 1.26, 1.28, and 1.32 Å. **s4** resides 27.1 kcal/mol below $O(^1D) + CO_2$, so that the adiabatic excitation energy of **s2** into the first excited singlet electronic state constitutes 20 kcal/mol. The **s3** → **s4** rearrangement takes place via C_s-symmetric transition state s-TS2 over a barrier of 17.7 and 11.1 kcal/mol relative to **s3** and $O(^1D) + CO_2$, respectively. Because the barrier at s-TS2 is rather high, the $^1A_2-^1A''$ PES is not expected to play a significant role in the $O(^1D) + CO_2 \Delta CO_3$ isotope exchange reaction. Complex **s3** can be formed, but isotope scrambling in this complex cannot occur unless it rearranges to **s4**, which cannot happen if the reaction collision energy is below 11.1 kcal/mol.

Two local minima have been found on the lowest triplet PES of CO_3. Isomer **t1** has a C_{2v}-symmetric structure ($^3B_2$) with the central carbon connected to three O atoms with one double and two single bonds. **t1** is 24.7 kcal/mol more stable than $O(^1D) + CO_2$ but lies ~23 kcal/mol higher than the $O(^3P) + CO_2$ asymptote. Dissociation of **t1** to the latter products occurs via transition state t-TS1, in which one of the single C−O bonds lengthens from 1.34 to 1.52 Å, the other shortens to 1.24 Å, and the OCO angle in the forming CO_2 fragment reaches 146.3°

versus 122.6° in **t1**, thus approaching 180°. The barrier at t-TS1 is calculated as 13.2 and 36.2 kcal/mol in the **t1** → $O(^3P) + CO_2$ and opposite directions, respectively. This result indicates that the $O(^3P) + CO_2 \rightarrow$ **t1** reaction can occur only with hyperthermal $O(^3P)$ atoms. The other isomer of triplet CO_3 is O=C−O−O, **t2** (C_s, $^3A''$). This structure lies 15.5 and 63.2 kcal/mol above $O(^1D) + CO_2$ and $O(^3P) + CO_2$, respectively. Therefore, **t2** is not likely to play any role in the $O(^1D) + CO_2$ reaction, although it is expected to be important for the reaction to form $CO + O_2$. We do not consider the $O(^1D) + CO_2 \rightarrow CO + O_2$ reaction here because it is much slower (the rate constant is ~10^{-18} cm^3 molecule^{-1} s^{-1} at 1700 K[53]) than the exchange reaction $O(^1D) + CO_2 \rightarrow O(^1D)/O(^3P) + CO_2$ with the rate constant of ~10^{-10} cm^3 molecule^{-1} s^{-1} at 300 K.[25] In addition to characterizing stationary points on the triplet PES, we have also located a minimum on the seam of crossing between the lowest singlet and triplet electronic states (MSX). Geometry optimization of MSX was carried out using the Lagrange multipliers method[54] at the CASSCF/6-311G(d) level. The structure of MSX appeared to be rather close to that of t-TS1, with a slightly longer distance (1.57 vs 1.52 Å in the transition state) for the forming/breaking CO bond. Thus, the $^3A'$ and $^1A'$ PESs cross each other (with the minimal energy) in the vicinity of transition state t-TS1, and the energy of MSX is close to that of the transition state. Interestingly, if hyperthermal $O(^3P)$ reacts with CO_2, MSX can be encountered before t-TS1.

Let us now compare relative energies of various species calculated at different levels of theory (see Table 1). MRCI+Q energies calculated with the 6-311+G(3df) and pvtz basis sets normally differ by less than 1 kcal/mol, except for the **s0** complex where the difference reaches ~6 kcal/mol. As compared to MRCI+Q/6-311+G(3df), CCSD(T) calculations with the same basis set regularly underestimate relative energies for most species by ~4 kcal/mol. This is related to the fact that the single-reference CCSD(T) method overestimates the singlet−triplet energy gap for the oxygen atom by 3.3 and 5.6 kcal/mol as compared to the MRCI+Q calculated value and experiment,[55] respectively. The wave function of $O(^1D)$ has a strong multi-reference character and cannot be properly described by a single-reference method, which causes the above-mentioned deviations. If we consider relative energies of various intermediates and transition states with respect to $O(^3P) + CO_2$, the differences between the CCSD(T) and MRCI+Q values are in the range of 0.9−2.3 kcal/mol, excluding $O(^1D) + CO_2$ and **s0**. The B3LYP method does not seem to be reliable for this system as the $O(^1D)−O(^3P)$ energy gap is underestimated by ~30 kcal/mol at this level. This leads to large deviations in relative energies for the CO_3 intermediates and transition states.

On the basis of the fact that the CCSD(T) relative energies with respect to $O(^3P) + CO_2$ are close to the MRCI+Q values, we can carry out CCSD(T) calculations with larger basis sets to estimate a more accurate energy of **s1**. The CCSD(T) method is much more efficient than MRCI in terms of computing demands. Moreover, it includes correlation from all valence electrons, while in the MRCI(16,13) calculations 2s lone pairs of oxygen atoms were excluded. Therefore, we performed CCSD(T) calculations with a series of correlation-consistent Dunning's basis sets pvtz, pvqz, and pv5z[48] and obtained the relative energy of **s1** with regards to $O(^3P) + CO_2$ as −0.47, −1.72, and −2.45 kcal/mol, respectively. Extrapolation of these results to the complete basis set limit[56] gives the energy of **s1** as −3.47 kcal/mol. Taking into account that the MRCI+Q relative energies for this species are ~0.9 kcal/mol higher than the CCSD(T) energies with the same basis sets (6-311+G(3df)

Theoretical Study of the O(^{1}D) + CO$_2$ Reaction

J. Phys. Chem. A, Vol. 108, No. 39, 2004 **7987**
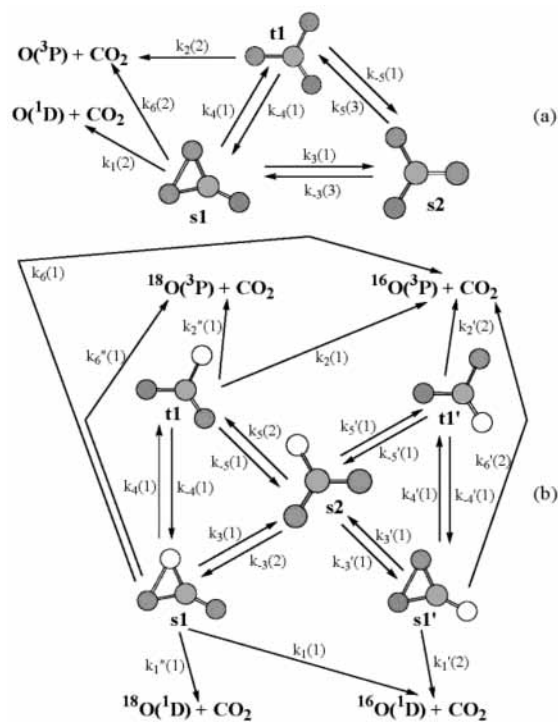
Figure 2. Kinetic schemes used for calculations of product branching ratios in the decomposition of the chemically activated CO$_3$ (intermediate **s1**) formed in the O(^{1}D) + CO$_2$ reaction: (a) no isotope labels, ^{16}O(^{1}D) + ^{44}CO$_2$ reaction; (b) isotope-labeled ^{18}O(^{1}D) + ^{44}CO$_2$ reaction, ^{18}O atoms are shown in white. The numbers in parentheses show reaction path degeneracies for each rate constant.

or pvtz), we can conclude that the best estimate for the energy of **s1** with respect to O(^{3}P) + CO$_2$ should be between −3.5 and −2.5 kcal/mol. Now, using the experimental energy gap between O(^{1}D) and O(^{3}P), 45.37 kcal/mol,[55] we find the best estimate for the relative energy of **s1** with respect to O(^{1}D) + CO$_2$ to be between −48.8 and −47.8 kcal/mol. Finally, if we take 48.8 kcal/mol as the energy gap at **s1** and the barrier at s-TS0 as 48.5 kcal/mol with respect to **s1** [as calculated at the MRCI+Q/6-311+G(3df) level)], then s-TS0 lies 0.3 kcal/mol below the O(^{1}D) + CO$_2$ reactants (see bold numbers in Figure 1). This result is consistent with a small negative activation energy observed in kinetic experiments for the O(^{1}D) + CO$_2$ reaction.[25] However, the use of the barrier height obtained at MRCI+Q/pvtz (49.2 kcal/mol) puts the transition state s-TS0 0.4 kcal/mol above the reactants. Therefore, we can only conclude here that either the barrier for the O(^{1}D) + CO$_2$ → CO$_3$ (**s1**) reaction is very low or the corresponding transition state lies slightly lower than the reactants. Even higher-level calculations such as MRCI+Q with full-valence active space extrapolated to the complete basis set limit can finally solve this question, but such calculations unfortunately are not feasible now.

Methods of Calculations of Rate Constants

Now we set out to calculate branching ratios of nonquenching isotope exchange/quenching isotope exchange in the O(^{1}D) + CO$_2$ ⇌ CO$_3$ → O(^{3}P)/O(^{1}D) + CO$_2$ reaction. To do that, we consider the chemically activated CO$_3$ intermediate **s1** produced in the O(^{1}D) + CO$_2$ collisions (assuming that the collision energy is sufficient to overcome the barrier at s-TS0) and compute rate constants for various dissociation and isomerization processes as illustrated in Figures 1 and 2. Because the barrier at s-TS2 is high (11.1 kcal/mol) and formation of the **s3** complex

on the first excited singlet PES is not expected to result in isotope exchange, we consider here only the lowest energy singlet and triplet PESs. For the reactions which involve species of the same multiplicity, **s1** $\xrightarrow{k_1}$ O(^{1}D) + CO$_2$ via s-TS0, **t1** $\xrightarrow{k_2}$ O(^{3}P) + CO$_2$ via t-TS1, and **s1** $\xrightarrow{k_3}$ **s2** and **s2** $\xrightarrow{k_{-3}}$ **s1** via s-TS1, we use standard RRKM theory (quasiequilibrium theory) to calculate the rate constants k_1, k_2, k_3, and k_{-3}. In RRKM theory,[57] a rate constant $k(E)$ at an internal energy E for a unimolecular reaction A* → A$^\#$ → P can be expressed as

$$k(E) = \frac{\sigma}{h} \cdot \frac{W^\#(E - E^\#)}{\rho(E)}$$

where σ is the reaction path degeneracy, h is Plank's constant, $W^\#(E - E^\#)$ denotes the total number of states for the transition state (activated complex) A$^\#$ with a barrier $E^\#$, $\rho(E)$ represents the density of states of the energized reactant molecule A*, and P is the product or products. We used the harmonic approximation to calculate the total number and density of states, and the saddle-point method[57] was employed for these computations. Vibrational frequencies used in the calculations were obtained at the CASSCF(16,13)/6-311+G(d) level of theory and are presented in Table S1 of the Supporting Information. The available internal energy of the intermediate **s1** was assumed to be equal to the well depth for this isomer (we took the 48.8 kcal/mol value as the best estimate) plus collision energy. For the other species, the available internal energies are less than that for **s1** by the amounts equal to their relative energies with respect to **s1** calculated at the MRCI+Q/6-311+G(3df) level (see Figure 1 and Table 1). The resulting rate constants k_1, k_2, k_3, and k_{-3} computed for various collision energies between 0 and 10 kcal/mol are shown in Table 2.

A more challenging task is to calculate reaction rate constants involving a change of the spin multiplicity, for instance, for the **s1** ⇌ **t1** (k_4/k_{-4}) and **s2** ⇌ **t1** (k_5/k_{-5}) rearrangements. Several approaches exist to address this problem, including nonadiabatic dynamical studies or nonadiabatic statistical rate theories.[27−35] For instance, the latter theories involve using a multiplicative "transmission factor" related to the spin−orbit coupling strength to correct the rate computed using standard transition state theory, where the minimum on the seam of crossing between two PESs (MSX) involved is treated like the transition state of adiabatic statistical methods. The density of states for the transition state in the TST (or RRKM) rate equation is then multiplied by the probability of hopping from one surface to the other. To a first approximation, this term can be calculated in a pseudo-one-dimensional way using either Landau−Zener theory or from WKB theory.[34,35] The rate constant is then expressed as

$$k(E) = \frac{\sigma}{h\rho(E)} \int_0^\infty dE_h \rho^{MSX}(E - E_h) p_{sh}(E_h)$$

Here, $\rho^{MSX}(E - E_h)$ is the density of states for the degrees of freedom within the crossing seam at the MSX, and E_h is the part of the available energy which is in the coordinate orthogonal to the seam. According to the Landau−Zener formula, the hopping probability $p_{sh}(E_h)$ is given by

$$p_{sh}^{Landau-Zeener}(E_h) = (1 + P)(1 - P)$$

$$P = \exp\left(\frac{-2\pi V_{12}^2}{h\Delta F} \sqrt{\frac{\mu_h}{2(E - E_{MSX})}}\right)$$

TABLE 2: Rate Constants (s⁻¹) for Various Isomerization and Dissociation Pathways on the CO₃ Singlet and Triplet Potential Energy Surfaces Calculated Using RRKM Theory[a]

$E_{collision}$ (kcal/mol)	k_1[b] $E^\# = 48.5$	$E^\# = 49.2$	k_2	k_3	k_{-3}
0	1.21×10^9		3.63×10^{12}	1.05×10^{13}	1.77×10^{13}
0.5	1.88×10^9	1.08×10^9	3.86×10^{12}	1.05×10^{13}	1.78×10^{13}
1	2.87×10^9	1.48×10^9	4.09×10^{12}	1.06×10^{13}	1.78×10^{13}
2	5.74×10^9	3.39×10^9	4.55×10^{12}	1.07×10^{13}	1.80×10^{13}
3	1.00×10^{10}	6.48×10^9	5.03×10^{12}	1.07×10^{13}	1.81×10^{13}
4	1.59×10^{10}	1.10×10^{10}	5.52×10^{12}	1.08×10^{13}	1.82×10^{13}
4.2	1.73×10^{10}	1.20×10^{10}	5.62×10^{12}	1.09×10^{13}	1.82×10^{13}
5	2.38×10^{10}	1.71×10^{10}	6.02×10^{12}	1.09×10^{13}	1.83×10^{13}
6	3.37×10^{10}	2.51×10^{10}	6.52×10^{12}	1.10×10^{13}	1.84×10^{13}
7	4.61×10^{10}	3.52×10^{10}	7.03×10^{12}	1.11×10^{13}	1.86×10^{13}
7.7	5.65×10^{10}	4.37×10^{10}	7.39×10^{12}	1.12×10^{13}	1.86×10^{13}
8	6.12×10^{10}	4.77×10^{10}	7.54×10^{12}	1.12×10^{13}	1.87×10^{13}
9	7.91×10^{10}	6.28×10^{10}	8.06×10^{12}	1.13×10^{13}	1.88×10^{13}
10	1.00×10^{11}	8.07×10^{10}	8.57×10^{12}	1.13×10^{13}	1.89×10^{13}

[a] Reaction path degeneracies shown in Figure 2a are taken into account. Available internal energies used in the RRKM calculations were computed as $E_{avail} = E_{collision} + 48.8$, where 48.8 kcal/mol is the best estimate of the potential energy well depth for the **s1** isomer relative to $O(^1D) + CO_2$. [b] Rate constant k_1 was calculated for two different values of the barrier height $E^\#$ at transition state s-TS0 with respect to **s1** obtained at the MRCI+Q/6-311+G(3df) and MRCI+Q/pvtz levels of theory.

In this expression, V_{12} is the spin−orbit coupling term at MSX, μ_h is the reduced mass for movement along the direction orthogonal to the crossing seam, and ΔF is the norm of the difference of the gradients on the two surfaces at MSX.

In the present study, in addition to the nonadiabatic transition state theory method described above, we also employ an alternative approach, which does not require the PESs involved to cross and MSX to exist. Our method is based on the theory of radiationless transitions.[36−44] In this theory, the rate constant for a radiationless transition (nonradiative decay) from a local minimum on one PES to another local minimum on a second PES is determined through the overlap between wave functions between these two structures. We adopt the adiabatic approximation, which allows the vibronic (i.e., electronic and vibrational) description of this process. The rate constant is then expressed as a product of the overlap of electronic wave functions (spin−orbit coupling term for the case of ISC) and that of vibrational wave functions (Franck−Condon factor):

$$W_{b \leftarrow a}(\omega_{ba}) = \frac{1}{\hbar^2}|V_{ISC}(b \leftarrow a)|^2 \int_{-\infty}^{\infty} dt\, e^{it\omega_{ba}} \prod_{l=1}^{N} G_l^{ba}(t)$$

where

$$G_l^{ba}(t) = \frac{2n_l^{ba} e^{it(\omega_l^a - \omega_l^b)/2}(e^{\hbar\omega_l^a/kT} - 1)}{\omega_l^a + \omega_l^b} \sqrt{\frac{\omega_l^a \omega_l^b}{f_l^{ba+} f_l^{ba-}}} \times$$

$$\exp\left\{ \frac{-\omega_l^a \omega_l^b (d_l^{ba})^2}{\hbar(\omega_l^a + \omega_l^b)} \times \frac{(1 + 2n_l^{ba}) - g_l^{ba+}}{f_l^{ba-}} \right\}$$

$$g_l^{ba\pm} = (n_l^{ba} + 1)e^{it\omega_l^b} \pm n_l^{ge} e^{-it\omega_l^b}$$

$$f_l^{ba\pm} = 1 \pm \frac{\omega_l^b - \omega_l^a}{\omega_l^b + \omega_l^a} g_l^{ba-}$$

$$n_l^{ba} = \frac{1}{e^{it(\omega_l^a - \omega_l^b) + \hbar\omega_l^a/kT} - 1}$$

In these equations, ω_{ba} is the energy gap between two local minima a and b on two different PESs, $V_{ISC(b \leftarrow a)}$ is the spin−orbit coupling term, $\{\omega_1^a, \omega_2^a, ..., \omega_N^a\}$ and $\{\omega_1^b, \omega_2^b, ..., \omega_N^b\}$ are

vibrational frequencies for the two local minima, and $\{d_1^{ba}, d_2^{ba}, ..., d_N^{ba}\}$ are normal mode displacements from one local minimum to the other. All of these quantities can be obtained from ab initio calculations. Effective temperature T corresponding to available internal energy E can be computed employing the equipartition theorem. The spin−orbit coupling is taken out of the integral in these calculations assuming it is a constant; the values of the spin−orbit coupling constants were computed at the equilibrium structures involved in the singlet−triplet transitions (see below). In the calculations of the Franck−Condon factor, we used the approximation of displaced and distorted harmonic oscillators and did not take into account a mixing between normal modes because this mixing (Duschinsky rotation) is not significant for the **s1** → **t1** and **s2** → **t1** transitions.

Using the approach described above, we computed the ISC rate constants **s1** → **t1** (k_4), **t1** → **s1** (k_{-4}), **s2** → **t1** (k_5), **t1** → **s2** (k_{-5}), which are shown in Table 3. It should be noted that for k_4 and k_{-4} Franck−Condon factors involve vibrational overlap between the **s1** and **t1** isomers, but they are computed at different effective temperatures because the available internal energies for the two species differ. Also, in the calculations of k_4, we used the spin−orbit coupling term obtained at the CASSCF/6-311G(d) level at the geometry of **s1**, while the spin−orbit coupling term obtained at the **t1** geometry was employed to compute k_{-4}. Similar statements can be made concerning the rate constants k_5 and k_{-5}. Thus, k_{-4} and k_{-5} include the same $V_{ISC}(b \leftarrow a)$ term and differ by their Franck−Condon factors. Rate constant k_6 for the dissociation of **s1** directly to the $O(^3P) + CO_2$ products on the triplet PES via MSX was computed using the nonadiabatic transition state theory with Landau−Zener hopping probability.

Rate Constants

As seen in Table 2, rate constant k_1 for the **s1** → $O(^1D) + CO_2$ dissociation process rapidly increases with a rise in the collision energy. The growth is nearly 2 orders of magnitude from $E_{col} = 0$ to 10 kcal/mol. This is due to the fact that the available energy is only slightly higher than the energy of the transition state s-TS0, so that the number of states for the transition state increases much faster than the density of states for **s1**. One can also see that k_1 values are sensitive to the barrier height used in the calculations, especially for low collision

TABLE 3: Franck−Condon Factors, Spin−Orbit Coupling Constants, and Intersystem Crossing Rate Constants for the s1 → t1, t1 → s1, s2 → t1, and t1 → s2 Transitions Calculated Using the Theory of Radiationless Transitions

(a) Franck−Condon Factors (cm^2 s^{-1})

$E_{collision}$, kcal/mol	**s1 → t1**	**t1 → s1**	**s2 → t1**	**t1 → s2**
0	7.14×10^7	6.16×10^7	4.33×10^7	1.34×10^8
0.5	7.14×10^7	6.19×10^7	4.34×10^7	1.32×10^8
1	7.14×10^7	6.23×10^7	4.35×10^7	1.30×10^8
2	7.14×10^7	6.31×10^7	4.37×10^7	1.28×10^8
3	7.14×10^7	6.37×10^7	4.39×10^7	1.25×10^8
4	7.14×10^7	6.43×10^7	4.41×10^7	1.23×10^8
4.2	7.14×10^7	6.45×10^7	4.41×10^7	1.23×10^8
5	7.14×10^7	6.49×10^7	4.43×10^7	1.21×10^8
6	7.15×10^7	6.54×10^7	4.45×10^7	1.20×10^8
7	7.15×10^7	6.59×10^7	4.47×10^7	1.18×10^8
7.7	7.15×10^7	6.63×10^7	4.49×10^7	1.17×10^8
8	7.15×10^7	6.64×10^7	4.49×10^7	1.17×10^8
9	7.15×10^7	6.68×10^7	4.51×10^7	1.16×10^8
10	7.15×10^7	6.72×10^7	4.53×10^7	1.15×10^8

(b) Spin−Orbit Coupling Constants (cm^{-1})

s1	**s2**	**t1**	**MSX**
5.5	26	14	63

(c) Intersystem Crossing Rate Constants (s^{-1})^a

E_{col}, kcal/mol	k_4 (s1 → t1)	k_{-4} (t1 → s1)	k_5 (s2 → t1)	k_{-5} (t1 → s2)	k_6 (MSX)
0	2.16×10^9	1.21×10^{10}	2.93×10^{10}	2.63×10^{10}	5.79×10^8
0.5	2.16×10^9	1.21×10^{10}	2.93×10^{10}	2.60×10^{10}	6.27×10^8
1	2.16×10^9	1.22×10^{10}	2.94×10^{10}	2.56×10^{10}	6.77×10^8
2	2.16×10^9	1.24×10^{10}	2.95×10^{10}	2.50×10^{10}	7.83×10^8
3	2.16×10^9	1.25×10^{10}	2.97×10^{10}	2.46×10^{10}	8.98×10^8
4	2.16×10^9	1.26×10^{10}	2.98×10^{10}	2.42×10^{10}	1.02×10^9
4.2	2.16×10^9	1.26×10^{10}	2.98×10^{10}	2.41×10^{10}	1.04×10^9
5	2.16×10^9	1.27×10^{10}	2.99×10^{10}	2.38×10^{10}	1.15×10^9
6	2.16×10^9	1.28×10^{10}	3.01×10^{10}	2.35×10^{10}	1.28×10^9
7	2.16×10^9	1.29×10^{10}	3.02×10^{10}	2.32×10^{10}	1.43×10^9
7.7	2.16×10^9	1.30×10^{10}	3.03×10^{10}	2.30×10^{10}	1.54×10^9
8	2.16×10^9	1.30×10^{10}	3.04×10^{10}	2.29×10^{10}	1.58×10^9
9	2.16×10^9	1.31×10^{10}	3.05×10^{10}	2.27×10^{10}	1.73×10^9
10	2.16×10^9	1.32×10^{10}	3.07×10^{10}	2.25×10^{10}	1.89×10^9

^{a} Symmetry factors (reaction path degeneracies) shown in Figure 2 were not included in the values shown here but were taken into account in the calculations of branching ratios. Intersystem crossing rate constants used for the calculations of branching ratios in the isotope-labeled system [Figure 2b], k_4', k_{-4}', k_5', k_{-5}', differ from k_4, k_{-4}, k_5, k_{-5}, respectively, only by the symmetry factors.

energies. We computed the rates for two $E^{\#}$ values, 48.5 and 49.2 kcal/mol, obtained at the MRCI+Q level of theory with the 6-311+G(3df) and pvtz levels, respectively. For the case of $E^{\#}$ = 49.2 kcal/mol, the reaction cannot take place at zero collision energy. For E_{col} = 0.5 kcal/mol, the k_1 value computed with the 48.5 kcal/mol barrier is a factor of 1.74 higher than that obtained with 49.2 kcal/mol. However, as the collision energy increases, this ratio eventually decreases to 1.15 at E_{col} = 10 kcal/mol.

For k_2, the available energy is at least 11.5 kcal/mol higher than the threshold value and the changes as the collision energy increases are less pronounced as compared to those for k_1. For instance, from E_{col} = 0 to 10 kcal/mol, k_2 rises a factor of only 2.36. Rate constants k_3 and k_{-3} are least sensitive to the reaction collision energy because they correspond to the low barrier **s1** ⇆ **s2** reactions and transition state s-TS1 lies 42.8 kcal/mol below O(^{1}D) + CO$_2$, so that the available energy is higher than the threshold value by at least this amount. As a result, k_3 and k_{-3} are high and show only a small 7−8% increase with E_{col}. It should also be noted that the k_3 and k_{-3} values are somewhat higher than the RRKM applicability limit of 10^{13} s^{-1} determined by the rate of intramolecular vibrational relaxation (IVR), which normally occurs on a picosecond scale. Therefore, some dynamic effects may be significant for the **s1** ⇆ **s2** isomerization.

Intersystem crossing rate constants k_4, k_{-4}, k_5, and k_{-5} (Table 3) are nearly independent of the collision energy. This result originates from the fact that the available energy is much higher (by at least ∼25 kcal/mol) than the threshold, which constitutes ∼22.5 kcal/mol for the **s1** → **t1** and **s2** → **t1** transitions and close to zero for the reverse rearrangements. k_5 values are about an order of magnitude higher than k_4 due to the higher value of the spin−orbit coupling term for the **s2** structure (26 vs 5.5 cm^{-1} for **s1**). The rates are proportional to the square of the spin−orbit coupling constants, while the difference in V_{ISC} is somewhat compensated by the higher Franck−Condon factor between **s1** and **t1** as compared to that between **s2** and **t1**.

Rate constants k_6 for the **s1** → MSX → O(^{3}P) + CO$_2$ process appear to be significantly lower than k_4 and especially k_5 (see Table 3). Despite the fact that V_{12} at MSX (63 cm^{-1}) is higher than those at **s1** and **s2**, the hopping probability is computed to be about 10^{-2} near MSX (at E_h close to and slightly higher than E_{MSX}), but it rapidly decreases when E_h increases—by a factor of 5 within 3 kcal/mol and by an order of magnitude within 10 kcal/mol. As a result, k_6 computed for the nonadiabatic process is ∼300 times lower than a rate constant for a hypothetical adiabatic process involving MSX as a transition state. Rate constants k_6 show a moderate increase with a rise of the available energy and change by a factor of ∼2.7 from E_{col} = 0 to 10 kcal/mol.

Branching Ratios in the $^{16}O(^1D) + {}^{44}CO_2$ Reaction

To compute branching ratios for the $O(^1D) + CO_2$ and $O(^3P) + CO_2$ products in the decomposition of chemically activated intermediate **s1** formed in the $O(^1D) + CO_2$ reaction at different collision energies between 0 and 10 kcal/mol, we used the calculated rate constants k_1-k_6 and kinetic scheme shown in Figure 2a. The kinetic master equations are then written as follows:

$$d[\mathbf{s2}]/dt = k_3[\mathbf{s1}] + k_{-5}[\mathbf{t1}] - (k_{-3} + k_5)[\mathbf{s2}]$$

$$d[\mathbf{t1}]/dt = k_4[\mathbf{s1}] + k_5[\mathbf{s2}] - (k_2 + k_{-4} + k_{-5})[\mathbf{t1}]$$

Using the steady-state approximation, $d[\mathbf{s2}]/dt = 0$ and $d[\mathbf{t1}]/dt = 0$, we express concentrations of the **s2** and **t1** intermediates in terms of [**s1**] and then calculate rate constants for the production of $O(^1D) + CO_2$ and $O(^3P) + CO_2$:

$$d[O(^1D) + CO_2]/dt = k_1[\mathbf{s1}]$$

$$d[O(^3D) + CO_2]/dt = k_6[\mathbf{s1}] + k_2[\mathbf{t1}]$$

which allows us to obtain the product branching ratios.

The results are shown in Table 5 (column *a*) and plotted in Figure 3a. As one can see, the $O(^3P) + CO_2$ products are dominant at low collision energies ($\sim$98% at $E_{col} = 0$), but the calculated branching ratio for $O(^1D) + CO_2$ rapidly increases with E_{col}. The branching ratios are sensitive to the barrier height $E^{\#}$ at t-TS0 with respect to **s1**. We carried out the calculation for two values of $E^{\#}$, 48.5 kcal/mol obtained at the MRCI+Q/6-311+G(3df) level and 49.2 kcal/mol (MRCI+Q/pvtz). The differences are not large for low collision energies but reach 5−6% at E_{col} greater than 3 kcal/mol. The $O(^1D) + CO_2$ product branching ratio becomes larger than that for $O(^3P) + CO_2$ at $E_{col} = 8$ and 9 kcal/mol for $E^{\#} = 48.5$ and 49.2 kcal/mol, respectively. The rapid growth of the $O(^1D) + CO_2$ relative product yield is due to the fast increase of rate constant k_1 when the available energy increases and is only slightly above the threshold energy $E^{\#}$ needed for the reaction to occur. Another interesting result is that the $O(^3P) + CO_2$ products are mostly produced via **t1**, that is, through the radiationless transition mechanism not involving the MSX; the radiationless transition rate constants are $5.3-5.7 \times 10^{10}$ s^{-1}. Only a small fraction of $O(^3P) + CO_2$ products (2−6%) are formed directly from **s1** via the MSX with rate constants for this process varying from 1.2×10^9 to 3.8×10^9 s^{-1} as a function of collision energy.

Branching Ratios in the $^{18}O(^1D) + {}^{44}CO_2$ Reaction: Comparison with Experiment

In the crossed-beam experiments,[3,4] relative yields were measured for isotope exchange with and without quenching in the $^{18}O(^1D) + {}^{44}CO_2$ reaction, that is, for the $^{16}O(^1D) + {}^{46}CO_2$ and $^{16}O(^3P) + {}^{46}CO_2$ products, which have a different mass from that of the reactants and can therefore be most easily detected. In our calculations including isotope labeling, we use the rate constants in Table 4 computed for isotope-labeled species and the kinetic scheme shown in Figure 2b. One can see that this scheme is more complex due to the presence of an ^{18}O atom. Rate constants are also somewhat different because of differences in vibrational frequencies, zero-point energies, and reaction path degeneracies. Table 5 (column *b*) shows computed branching ratios for the four possible products, $^{16}O(^1D) + {}^{46}CO_2$, $^{18}O(^1D) + {}^{44}CO_2$, $^{16}O(^3P) + {}^{46}CO_2$, and $^{18}O(^3P) + {}^{44}CO_2$. Only the $^{16}O(^1D)$ and $^{16}O(^3P)$ are observable

TABLE 4: Rate Constants (s^{-1}) for Various Isomerization and Dissociation Pathways on the Singlet and Triplet Potential Energy Surfaces of Isotope-Labeled CO$_3$ Calculated Using RRKM Theory^a

E_{col} kcal/mol	$k_1{}^b$ 48.5	$k_1{}^b$ 49.2	$k_1'{}^b$ 48.5	$k_1'{}^b$ 49.2	$k_1''{}^b$ 48.5	$k_1''{}^b$ 49.2	k_2	k_2'	k_2''	k_3	k_3'	k_{-3}	k_{-3}'
0	5.71×10^8	5.00×10^8	1.13×10^9	1.02×10^9	5.35×10^8	5.15×10^8	1.80×10^{12}	3.57×10^{12}	1.78×10^{12}	1.02×10^{13}	1.04×10^{13}	1.16×10^{13}	5.86×10^{12}
0.5	8.95×10^8	7.03×10^8	1.78×10^9	1.39×10^9	8.41×10^8	6.59×10^8	1.91×10^{12}	3.80×10^{12}	1.89×10^{12}	1.03×10^{13}	1.05×10^{13}	1.16×10^{13}	5.89×10^{12}
1	1.36×10^9		2.71×10^9		1.29×10^9		2.03×10^{12}	4.02×10^{12}	2.01×10^{12}	1.03×10^{13}	1.05×10^{13}	1.16×10^{13}	5.91×10^{12}
2	2.74×10^9	1.61×10^9	5.48×10^9	3.21×10^9	2.63×10^9	1.54×10^9	2.26×10^{12}	4.49×10^{12}	2.24×10^{12}	1.04×10^{13}	1.06×10^{13}	1.17×10^{13}	5.95×10^{12}
3	4.79×10^9	3.09×10^9	9.61×10^9	6.19×10^9	4.63×10^9	2.97×10^9	2.50×10^{12}	4.96×10^{12}	2.47×10^{12}	1.05×10^{13}	1.07×10^{13}	1.18×10^{13}	5.99×10^{12}
4	7.64×10^9	5.24×10^9	1.54×10^{10}	1.05×10^{10}	7.41×10^9	5.07×10^9	2.74×10^{12}	5.45×10^{12}	2.71×10^{12}	1.06×10^{13}	1.08×10^{13}	1.19×10^{13}	6.03×10^{12}
4.2	8.31×10^9	5.76×10^9	1.67×10^{10}	1.16×10^{10}	8.07×10^9	5.58×10^9	2.79×10^{12}	5.54×10^{12}	2.76×10^{12}	1.06×10^{13}	1.08×10^{13}	1.19×10^{13}	6.04×10^{12}
5	1.14×10^{10}	8.19×10^9	2.30×10^{10}	1.65×10^{10}	1.11×10^{10}	7.95×10^9	2.99×10^{12}	5.94×10^{12}	2.96×10^{12}	1.07×10^{13}	1.09×10^{13}	1.20×10^{13}	6.07×10^{12}
6	1.62×10^{10}	1.21×10^{10}	3.28×10^{10}	2.43×10^{10}	1.58×10^{10}	1.17×10^{10}	3.24×10^{12}	6.44×10^{12}	3.21×10^{12}	1.08×10^{13}	1.09×10^{13}	1.20×10^{13}	6.11×10^{12}
7	2.22×10^{10}	1.70×10^{10}	4.49×10^{10}	3.42×10^{10}	2.17×10^{10}	1.65×10^{10}	3.49×10^{12}	6.94×10^{12}	3.46×10^{12}	1.09×10^{13}	1.10×10^{13}	1.21×10^{13}	6.15×10^{12}
7.7	2.73×10^{10}	2.11×10^{10}	5.51×10^{10}	4.26×10^{10}	2.66×10^{10}	2.06×10^{10}	3.67×10^{12}	7.30×10^{12}	3.64×10^{12}	1.09×10^{13}	1.11×10^{13}	1.22×10^{13}	6.18×10^{12}
8	2.95×10^{10}	2.30×10^{10}	5.97×10^{10}	4.65×10^{10}	2.89×10^{10}	2.25×10^{10}	3.75×10^{12}	7.45×10^{12}	3.71×10^{12}	1.09×10^{13}	1.11×10^{13}	1.22×10^{13}	6.18×10^{12}
9	3.82×10^{10}	3.03×10^{10}	7.73×10^{10}	6.13×10^{10}	3.74×10^{10}	2.96×10^{10}	4.01×10^{12}	7.97×10^{12}	3.97×10^{12}	1.10×10^{13}	1.12×10^{13}	1.23×10^{13}	6.22×10^{12}
10	4.84×10^{10}	3.90×10^{10}	9.80×10^{10}	7.89×10^{10}	4.74×10^{10}	3.82×10^{10}	4.26×10^{12}	8.48×10^{12}	4.22×10^{12}	1.11×10^{13}	1.13×10^{13}	1.23×10^{13}	6.25×10^{12}

^{a} Reaction path degeneracies shown in Figure 2b are taken into account. ^{b} Rate constants k_1, k_1', and k_1'' were calculated for two different values of the barrier height $E^{\#}$ at transition state s-TS0.

Theoretical Study of the O(^{1}D) + CO$_2$ Reaction

J. Phys. Chem. A, Vol. 108, No. 39, 2004 **7991**

TABLE 5: Branching Ratios (%) for O(^{1}D) and O(^{3}P) Products Calculated for Two Different Values of the Barrier Height $E^{\#}$ at Transition State s-TS0

E_{col} kcal/mol	$E^{\#}$ = 48.5 kcal/mol						$E^{\#}$ = 49.2 kcal/mol					
	a		b				a		b			
	O(^{1}D)	O(^{3}P)	^{16}O(^{1}D)	^{18}O(^{1}D)	^{16}O(^{3}P)	^{18}O(^{3}P)	O(^{1}D)	O(^{3}P)	^{16}O(^{1}D)	^{18}O(^{1}D)	^{16}O(^{3}P)	^{18}O(^{3}P)
0	2.17	97.83	1.36	0.64	65.49	32.50						
0.5	3.33	96.67	2.11	1.00	64.76	32.14	1.93	98.07	1.21	0.62	65.61	32.56
1	4.95	95.05	3.14	1.50	63.73	31.63	2.62	97.38	1.65	0.78	65.20	32.36
2	9.37	90.63	5.99	2.89	60.90	30.23	5.75	94.25	3.65	1.75	63.22	31.38
3	15.11	84.89	9.72	4.72	57.18	28.39	10.33	89.67	6.60	3.20	60.28	29.92
4	21.91	78.09	14.17	6.90	52.74	26.19	16.17	83.83	10.41	5.06	56.48	28.05
4.2	23.36	76.64	15.13	7.37	51.78	25.71	17.47	82.53	11.26	5.48	55.64	27.62
5	29.29	70.71	19.05	9.30	47.87	23.77	22.94	77.06	14.86	7.24	52.05	25.85
6	36.75	63.25	24.01	11.74	42.93	21.32	30.15	69.85	19.63	9.59	47.30	23.49
7	44.04	55.96	28.88	14.15	38.06	18.91	37.52	62.48	24.53	12.00	42.41	21.06
7.7	48.81	51.19	32.09	15.74	34.85	17.32	42.50	57.50	27.86	13.65	39.08	19.41
8	50.75	49.25	33.39	16.39	33.55	16.67	44.55	55.45	29.23	14.33	37.71	18.73
9	56.88	43.12	37.53	18.44	29.41	14.62	51.16	48.84	33.68	16.53	33.27	16.53
10	62.24	37.76	41.14	20.25	25.79	12.82	57.07	42.93	37.65	18.51	29.28	14.55

^{a} Decomposing chemically activated intermediate **s1** is formed in the ^{16}O(^{1}D) + ^{44}CO$_2$ reaction and does not have isotope labels. ^{b} Branching ratios of ^{16}O(^{1}D) + ^{46}CO$_2$, ^{18}O(^{1}D) + ^{44}CO$_2$, ^{16}O(^{3}P) + ^{46}CO$_2$, and ^{18}O(^{3}P) + ^{44}CO$_2$ produced from decomposing chemically activated intermediate **s1** formed in the ^{18}O(^{1}D) + ^{44}CO$_2$ reaction.

in the crossed-beam experiment. The relative branching ratios ^{16}O(^{1}D)/[total ^{16}O] and ^{16}O(^{3}P)/[total ^{16}O] can be easily computed from the data presented in Table 5 and are plotted in Figure 3b. In general, the relative branching ratio for the ^{16}O(^{1}D) + ^{46}CO$_2$ channel in the ^{18}O(^{1}D) + ^{44}CO$_2$ reaction is slightly lower than (but is within 1% of) the branching ratio for the ^{16}O(^{1}D) + ^{44}CO$_2$ channel in the ^{16}O(^{1}D) + ^{44}CO$_2$ reaction. The differences are mostly due to lower vibrational frequencies for the ^{62}CO$_3$ intermediates, which result in higher densities of states for the reactants and correspondingly somewhat lower rate constants for their decomposition (especially k_1). On the other hand, the rates for intersystem crossing critical for the overall production rate of O(^{3}P) + CO$_2$ are not sensitive (at least within our approximations) to isotope labeling in CO$_3$. As a result, the relative yield of ^{16}O(^{3}P) + ^{46}CO$_2$ in the ^{18}O(^{1}D) + ^{44}CO$_2$ reaction is slightly higher than the branching ratio for ^{16}O(^{3}P) + ^{44}CO$_2$ in the ^{16}O(^{1}D) + ^{44}CO$_2$ reaction.

To evaluate the percentage of the incoming O(^{1}D), which are incorporated into the product CO$_2$ molecules after the exchange reaction with and without quenching, we calculated the overall branching ratios of ^{44}CO$_2$ [produced with ^{18}O(^{1}D) or ^{18}O(^{3}D)] and ^{46}CO$_2$ [with ^{16}O(^{1}D) or ^{16}O(^{3}O)] in the ^{18}O(^{1}D) + ^{44}CO$_2$ reaction. These branching ratios are 33.06−33.18% and 66.94−66.82%, respectively; the relative yield of the ^{44}CO$_2$ product slightly increases and that of ^{46}CO$_2$ correspondingly decreases with an increase of the collision energy. Thus, our results confirm that isotope exchange occurs at a near-statistical rate and approximately two-thirds of incoming O atoms are incorporated into the product carbon dioxide molecules. From the data in Table 5, we can also compute the ^{16}O(^{1}D)/^{18}O(^{1}D) and ^{16}O(^{3}P)/^{18}O(^{3}P) branching ratios for different collision energies (see Table 6), which describe the kinetic isotope effect (KIE) in the ^{18}O(^{1}D) + ^{44}CO$_2$ reaction. For O(^{3}P), the ratios are close to the statistical value of 2.0 ranging from 2.015 for zero collision energy to 2.012 for E_{col} = 10 kcal/mol. On the other hand, the ^{16}O(^{1}D)/^{18}O(^{1}D) branching ratios deviate from the statistical value more significantly and vary from 2.11 to 2.03, as the collision energy increases from 0 to 10 kcal/mol.

Also shown in Figure 3b are the experimental measurements performed for two collision energies of 4.2 and 7.7 kcal/mol.[3,4] The best agreement of the calculated branching ratios is obtained with $E^{\#}$ = 49.2 kcal/mol. In this case, theoretical branching ratios agree with experiment to within 1% for E_{col} = 4.2 kcal/mol,

but for E_{col} = 7.7 kcal/mol the computed branching ratio of ^{16}O(^{1}D) + ^{46}CO$_2$ overestimates the experimental value by ~9%. For $E^{\#}$ = 48.5 kcal/mol, the deviations of theoretical values from experiment are larger, ~7% and ~15% at E_{col} = 4.2 and 7.7 kcal/mol, respectively. Apparently, the theoretical branching ratio for O(^{3}P) + CO$_2$ (isotope exchange with quenching) falls faster and that for O(^{1}D) +CO$_2$ (isotope exchange without quenching) rises more rapidly with E_{col} than the experimental values do.

Several reasons could be behind these deviations. First, the rate constants for the production of O(^{1}D) + CO$_2$ can be overestimated due to underestimation of the barrier height $E^{\#}$ at s-TS0. However, this is not likely because the thermal rate constant measured for the O(^{1}D) + CO$_2$ reaction exhibits a slightly negative temperature dependence,[25] indicating that the transition state energy (if such a TS exists at all) should be lower than the energy of the reactants. In Figure 4, we plotted the experimental rates of the O(^{1}D) +CO$_2$ reaction and theoretical high-pressure-limit rate constants computed using transition state theory with relative energies of s-TS0 taken as −0.3 and −0.6 kcal/mol, respectively, with respect to the O(^{1}D) + CO$_2$ reactants, that is, 48.5 and 48.2 kcal/mol relative to **s1**. One can see that the best agreement is found for $E^{\#}$ = 48.2 kcal/mol, while the rates computed with $E^{\#}$ = 48.5 kcal/mol underestimate the experimental values by a factor of 1.8−2.1. Moreover, a positive temperature dependence is found if the thermal rate is calculated with $E^{\#}$ = 49.2 kcal/mol (assuming the well depth at **s1** to be 48.8 kcal/mol). Although the computations of thermal rate constants are rather approximate—they are carried out for the high-pressure limit and do not take into account possible formation of the **s0** and **s3** complexes—they still illustrate that the barrier height at t-TS0 is not likely to be underestimated in our calculations.

Hence, a more likely reason for the deviation of the theoretical branching ratios from experiment is underestimation of rate constants leading to the production of O(^{3}P), especially at high collision energy. Because the ISC rates (k_4 and k_5) do not show a significant dependence on the available energy, the rate k_6 for the reaction through MSX (**s1** → MSX → O(^{3}P) + CO$_2$) is likely to be underestimated. This observation is in line with the results of previous theoretical calculations using the nonadiabatic transition state theory, which showed that the one-dimensional handling of the surface hopping probability often gives rate

(a)

(b)
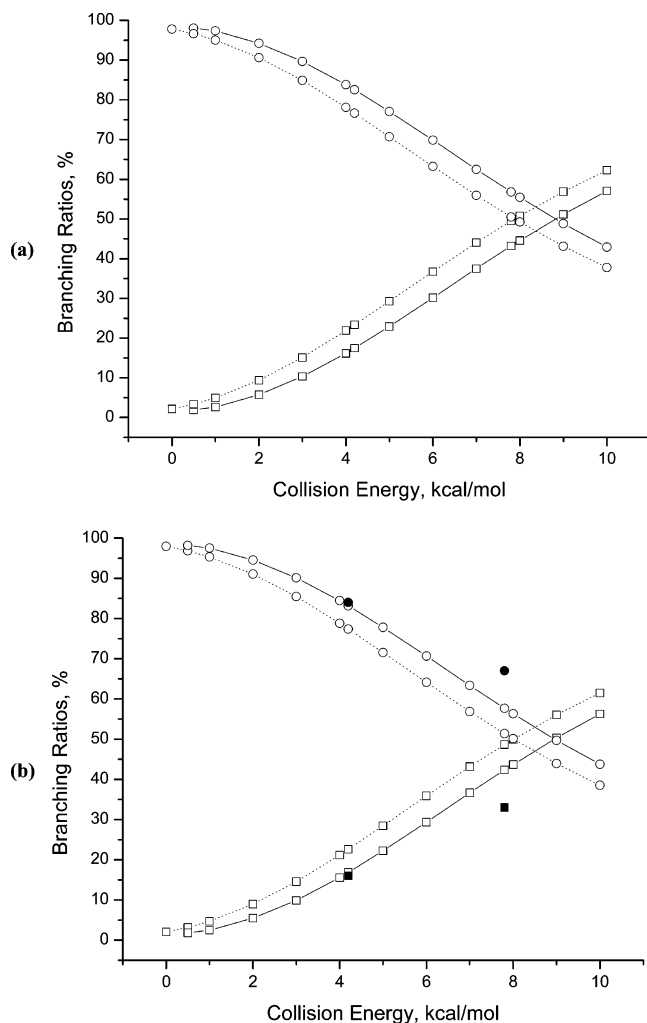
Figure 3. Branching ratios in decomposition of chemically activated CO_3 formed in the $O(^1D) + CO_2$ reaction as functions of the collision energy. The curves marked with open squares and open circles show the branching ratios of the $O(^1D) + CO_2$ and $O(^3P) + CO_2$ products, respectively. Closed squares and circles show experimental branching ratios from ref 4. Theoretical branching ratios were calculated for two different values of the barrier height $E^{\#}$ at transition state s-TS0 with respect to **s1** obtained at the MRCI+Q/6-311+G(3df) (48.5 kcal/mol, dotted curves) and MRCI+Q/pvtz (49.2 kcal/mol, solid curves) levels of theory. Plot a shows branching ratios for the $^{16}O(^1D) + ^{44}CO_2$ reaction without isotope labels. Plot b shows the relative branching ratios for the $^{16}O(^1D) + ^{46}CO_2$ and $^{16}O(^3P) + ^{46}CO_2$ products for the $^{18}O(^1D) + ^{44}CO_2$ reaction, that is, $^{16}O(^1D)/[\text{total }^{16}O]$ and $^{16}O(^3P)/[\text{total}$ $^{16}O]$, respectively, which are observable in experiment.

constants 1−2 orders of magnitude lower than experimental values;[28,35] extensive multidimensional nonadiabatic dynamical studies are required to improve theoretical treatment of this rate constant.[58] Another source for the deviations could be non-statistical (non-RRKM) redistribution of energy in the CO_3 intermediates. For instance, the branching ratios appear to be sensitive to the **s1 → s2** and **s2 → s1** rate constants, which are close to the RRKM applicability limit. If we fix the k_3 and k_{-3} values at exactly 10^{13}, the calculated yield of $O(^3P)$ increases because ISC mostly takes place through **s2** ($k_5 > k_4$). Therefore, if the **s2 → s1** rate (k_{-3}) is lowered, **s2** survives longer and the probability for the system to end up on the triplet PES is higher. Thus, the branching ratio depends on how long the system will be spending in the vicinity of the **s2** potential well as compared to **s1**. This could be a source for a non-RRKM behavior.

Despite the notable deviation from experiment at higher collision energies, our calculated branching ratios correctly
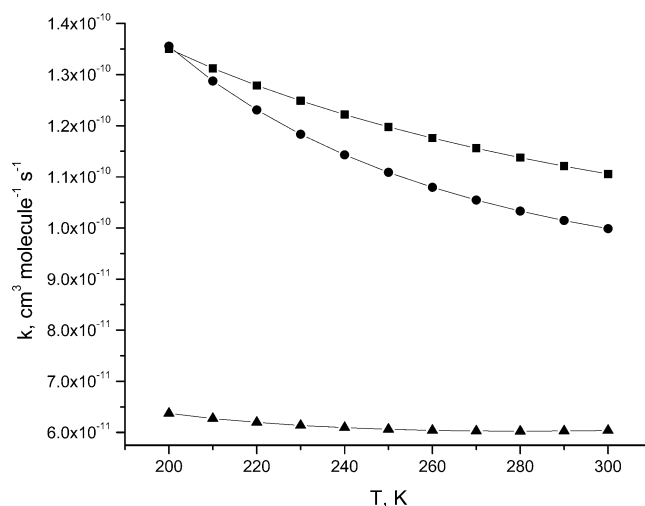
Figure 4. Calculated and experimental thermal rate constants for the $O(^1D) + CO_2$ reaction. The curve marked with closed squares shows experimental rate constants from ref 25. The curves marked with closed triangles and circles show rate constants calculated using the transition state theory (high-pressure limit rates) with relative energies of s-TS0 taken as −0.3 and −0.6 kcal/mol, respectively, with regards to the $O(^1D) + CO_2$ reactants.

TABLE 6: Branching Ratios $^{16}O(^1D)/^{18}O(^1D)$ and $^{16}O(^3P)/$ $^{18}O(^3P)$ Calculated for Different Collision Energies

E_{col}, kcal/mol	$^{16}O(^1D)/^{18}O(^1D)$	$^{16}O(^3P)/^{18}O(^3P)$
0	2.111	2.015
0.5	2.108	2.015
1	2.093	2.015
2	2.071	2.015
3	2.060	2.014
4	2.053	2.014
4.2	2.052	2.014
5	2.048	2.014
6	2.044	2.013
7	2.041	2.013
7.7	2.039	2.013
8	2.038	2.013
9	2.035	2.012
10	2.031	2.012

reproduce the experimental trend and quantitatively agree with experiment at $E_{col} = 4.2$ kcal/mol. Therefore, the results predicted for the lower collision energies are likely to be reliable. It should also be noted that theory would not be able to reproduce experimental branching ratios for isotope exchange/ quenching if one takes into account only the **s1 → MSX →** $O(^3P) + CO_2$ reaction channel via MSX and not considering radiationless transitions **s1 → t1** and **s2 → t1**, which play a dominant role in ISC, especially at low E_{col}.

Conclusions

Ab initio multireference configuration interaction calculations for the CO_3 system demonstrate that the $O(^1D) + CO_2$ reaction involves at least two PESs corresponding to singlet and triplet electronic states. The reaction starts from the formation of an $O-CO_2$ complex **s0**, which then isomerizes to a cyclic O= (CO_2) structure **s1** over a barrier at s-TS0. The best estimate for the relative energy of s-TS0 is 0.3 kcal/mol below the reactants. The cyclic isomer **s1**, which is predicted to lie 48.8 kcal/mol lower in energy than $O(^1D) + CO_2$, can in turn rearrange to a D_{3h} structure **s2**, only slightly higher in energy. The isomers **s1** and **s2** formed in the reaction possess high internal energy (chemically activated) and can decompose into the initial reactants. If the attacking oxygen atom is isotope-

Theoretical Study of the O(^{1}D) + CO$_2$ Reaction

J. Phys. Chem. A, Vol. 108, No. 39, 2004 **7993**

labeled, isotope exchange can occur due to the symmetry properties of the **s1** and **s2** isomers. Alternatively, **s1** and **s2** can undergo singlet−triplet intersystem crossing to form the triplet isomer **t1**, which can dissociate to O(^{3}P) + CO$_2$, overcoming a barrier at t-TS1. The triplet products can also be formed directly from **s1** through a minimum on the seam of crossing of the singlet and triplet PESs, which is found in the vicinity of the transition state t-TS1. On the first excited singlet surface, O(^{1}D) and CO$_2$ can form a strongly bound complex **s3** (^{1}A$_2$). However, the barrier for isomerization of this complex into excited isomer **s4** (^{1}A″) is high (11 kcal/mol relative to the initial reactants), and the excited singlet PES is not likely to contribute to isotope exchange at collision energies lower than 11 kcal/mol.

When the O(^{1}D) + CO$_2$ reaction initially produces chemically activated **s1**, the branching ratios for the O(^{1}D) + CO$_2$ and O(^{3}P) + CO$_2$ products depend on the dissociation (k_1 and k_2), isomerization (k_3 and k_{-3}), and ISC ($k_{4/-4}$, $k_{5/-5}$, and k_6) rate constants. The formation of the triplet products mostly occurs through the **s2** → **t1** radiationless transition, which has a rate constant nearly independent of the available energy. The contribution of the **s1** → MSX → O(^{3}P) + CO$_2$ process involving the crossing seam is much less significant, only 2−6%. Due to the fact that the rate constant for the **s1** → s-TS0 → O(^{1}D) + CO$_2$ dissociation on the singlet PES rapidly increases with available energy (and therefore with collision energy), the calculated branching ratio for the O(^{1}D) + CO$_2$ products also increases from 2% at zero collision energy to 57% at E_{col} = 10 kcal/mol. In the isotope-labeled ^{18}O(^{1}D) + ^{44}CO$_2$ reaction, the calculated relative branching ratios ^{16}O(^{1}D)/[total ^{16}O] observable in experiment are found to be slightly lower than (but within 1% of) the branching ratios for O(^{1}D) + CO$_2$ in the ^{16}O(^{1}D) + ^{44}CO$_2$ reaction without isotope labels. The computed relative branching ratios for ^{16}O(^{1}D) and ^{16}O(^{3}P) at E_{col} = 4.2 and 7.7 kcal/mol, 17/83 and 42/58, agree reasonably well with the experimental values of 16/84 and 33/67, respectively. The calculations also reproduce the qualitative trend with E_{col}, that is, an increase of the relative yield of isotope exchange without quenching when the collision energy grows. The calculated overall branching ratios of ^{44}CO$_2$ and ^{46}CO$_2$ confirm that the attacking O(^{1}D) atom can be incorporated into the product CO$_2$ molecule with a near-statistical probability of about $^2/_3$. On the other hand, KIE is displayed in the fact that the ^{16}O(^{1}D)/^{18}(^{1}D) branching ratio deviates for the statistical value of 2.0 and varies from 2.11 to 2.03 as collision energy increases, while the ^{16}O(^{3}P)/^{18}(^{3}P) ratio remains close to 2.0. The discrepancy of the O(^{1}D)/O(^{3}P) branching ratios from experiment at the higher E_{col} is attributed to an underestimation of the surface-hopping rate constant k_6 by the nonadiabatic transition state theory approach. Meanwhile, our results clearly demonstrate that the theory of radiationless transitions can be successfully employed to compute rate constants for intersystem crossing with reasonable accuracy using ab initio energies, geometric structures, vibrational normal modes and frequencies, and spin−orbit coupling constants as input data. Therefore, this approach, in combination with ab initio and RRKM calculations, can have broad applications for theoretical studies of rate constants and branching ratios of chemical reactions involving a change of electronic multiplicity.

Supporting Information Available: Vibrational frequencies (cm^{-1}) for different isotopologues of various intermediates and transition states on the singlet and triplet potential energy surfaces of CO$_3$ calculated at the CASSCF(16,13)/6-311G(d) level of theory (Table S1). This material is available free of charge via the Internet at http://pubs.acs.org.

References and Notes

(1) Yung, Y. L.; Lee, A. Y. T.; Irion, F. W.; DeMore, W. B.; Wen, J. *J. Geophys. Res., D: Atmos.* **1997**, *102*, 10857.

(2) Yung, Y. L.; Demore, W. B.; Pinto, J. P. *Geophys. Res. Lett.* **1991**, *18*, 13.

(3) Perri, M. J.; Van Wyngarden, A. L.; Boering, K. A.; Lin, J. J.; Lee, Y. T. *J. Chem. Phys.* **2003**, *119*, 8213.

(4) Perri, M. J.; Van Wyngarden, A. L.; Boering, K. A.; Lin, J. J.; Lee, Y. T. *J. Phys. Chem. A* **2004**, *108*, 7995.

(5) Gamo, T.; Tsutsumi, M.; Sakai, H.; Nakazawa, T.; Tanaka, M.; Honda, H.; Kubo, H.; Itoh, T. *Tellus B* **1989**, *41*, 127.

(6) Thiemens, M. H.; Jackson, T.; Mauersberger, K.; Schueler, B.; Morton, J. *Geophys. Res. Lett.* **1991**, *18*, 669.

(7) Thiemens, M. H.; Jackson, T. L.; Zipf, E. C.; Erdman, P. W.; Vanegmond, C. *Science* **1995**, *270*, 969.

(8) Thiemens, M. H.; Jackson, T. L.; Brenninkmeijer, C. A. M. *Geophys. Res. Lett.* **1995**, *22*, 255.

(9) Alexander, B.; Vollmer, M. K.; Jackson, T. L.; Weiss, R. F.; Thiemens, M. H. *Geophys. Res. Lett.* **2001**, *28*, 4103.

(10) Lammerzahl, P.; Rockmann, T.; Brenninkmeijer, C. A. M.; Krankowsky, D.; Mauersberger, K. *Geophys. Res. Lett.* **2002**, *29*, 1582.

(11) Boering, K. A.; Jackson, T.; Hoag, K.; Cole, A. S.; Perri, M. J.; Thiemens, M. H.; Atlas, E. *Geophys. Res. Lett.* **2004**, *31*, L03109.

(12) (a) Mauersberger, K. *Geophys. Res. Lett.* **1987**, *14*, 80. (b) Schueler, B.; Morton, J.; Mauersberger, K. *Geophys. Res. Lett.* **1990**, *17*, 1295. (c) Krankowsky, D.; Lammerzahl, P.; Mauersberger, K. *Geophys. Res. Lett.* **2000**, *27*, 2593.

(13) Mauersberger, K.; Erbacher, B.; Krankowsky, D.; Gunther, J.; Nickel, R. *Science* **1999**, *283*, 370.

(14) (a) Gao, Y. Q.; Marcus, R. A. *Science* **2001**, *293*, 259. (b) Gao, Y. Q.; Marcus, R. A. *J. Chem. Phys.* **2002**, *116*, 5913. (c) Gao, Y. Q.; Chen, W. C.; Marcus, R. A. *J. Chem. Phys.* **2002**, *117*, 1536.

(15) Baulch, D. L.; Breckenridge, W. H. *Trans. Faraday Soc.* **1966**, *62*, 2768.

(16) Hoag, K. J.; Boering, K. A.; Still, C. J.; Fung, I. Y.; Randerson, J. T. *EOS Trans. Am. Geophys. Union* **2002**, *83*, Fall Meet. Suppl., Abstract B71A-0707.

(17) (a) Luz, B.; Barkan, E.; Bender, M. L.; Thiemens, M. H.; Boering, K. A. *Nature* **1999**, *400*, 547. (b) Blunier, T.; Barnett, B.; Bender, M. L.; Hendricks, M. B. *Global Biogeochem. Cycles* **2002**, *16*, doi: 10.1029/2001GV001460.

(18) Atreya, S. K.; Gu, Z. G. *Adv. Space Res.* **1995**, *16*, 57.

(19) Yung, Y. L.; DeMore, W. B. *Photochemistry of Planetary Atmospheres*; Oxford University Press: Oxford, 1999.

(20) Bogard, D. D.; Clayton, R. N.; Marti, K.; Owen, T.; Turner, G. *Space Sci. Rev.* **2001**, *96*, 425.

(21) Moroz, V. I. *Adv. Space Res.* **1998**, *22*, 449.

(22) Galimov, E. M. *Dokl. Akad. Nauk* **1997**, *355*, 382.

(23) Wine, P. H.; Ravishankara, A. R. *Chem. Phys. Lett.* **1981**, *77*, 103.

(24) Young, R. A.; Black, G.; Slanger, T. G. *J. Chem. Phys.* **1968**, *49*, 4758.

(25) (a) Davidson, J. A.; Sadowski, C. M.; Schiff, H. I.; Streit, G. E.; Howard, C. J.; Jennings, D. A.; Schmeltekopf, A. L. *J. Chem. Phys.* **1976**, *64*, 57. (b) Streit, G. E.; Howard, C. J.; Schmeltekopf, A. L.; Davidson, J. A.; Schiff, H. I. *J. Chem. Phys.* **1976**, *65*, 4761. Sander, S. P.; Finlayson-Pitts, B. J.; Friedl, R. R. Jet Propulsion Laboratory, JPL Publication 02-25, Pasadena, CA, 2002.

(26) Froese, R. D. J.; Goddard, J. D. *J. Phys. Chem.* **1993**, *97*, 7484.

(27) Lorquet, J. C.; Leyh-Nihant, B. *J. Phys. Chem.* **1988**, *92*, 4778.

(28) Cui, Q.; Morokuma, K.; Bowman, J. M.; Klippenstein, S. J. *J. Chem. Phys.* **1999**, *110*, 9469.

(29) Aschi, M.; Grandinetti, F. *J. Chem. Phys.* **1999**, *111*, 6759.

(30) Harvey, J. N.; Grimme, S.; Woeller, M.; Peyerimhoff, S. D.; Danovich, D.; Shaik, S. *Chem. Phys. Lett.* **2000**, *322*, 358.

(31) de Moraes, P. R. P.; Linnert, H. V.; Aschi, M.; Riveros, J. M. *J. Am. Chem. Soc.* **2000**, *122*, 10133.

(32) Aschi, M.; Largo, A. *Chem. Phys.* **2001**, *265*, 251.

(33) Marks, A. J. *J. Chem. Phys.* **2001**, *114*, 1700.

(34) Harvey, J. N.; Aschi, M. *Phys. Chem. Chem. Phys.* **1999**, *1*, 5555.

(35) Harvey, J. N.; Aschi, M. *Faraday Discuss.* **2003**, *124*, 129.

(36) Lin, S. H. *Proc. R. Soc. London, Ser. A* **1976**, *352*, 57.

(37) (a) Lin, S. H. *J. Chem. Phys.* **1966**, *44*, 3759. (b) Lin, S. H.; Bersohn, R. *J. Chem. Phys.* **1968**, *48*, 2732.

(38) Lin, S. H. *J. Chem. Phys.* **1973**, *58*, 5760.

(39) (a) Englman, R.; Jortner, J. *Mol. Phys.* **1970**, *18*, 145. (b) Freed, K. F.; Jortner, J. *J. Chem. Phys.* **1970**, *52*, 1272.

(40) Nitzan, A.; Jortner, J. *J. Chem. Phys.* **1971**, *55*, 1355.

(41) Siebrand, W. *J. Chem. Phys.* **1971**, *54*, 363.

(42) Fischer, S. F. *Chem. Phys. Lett.* **1971**, *11*, 577.

(43) Heller, D. F.; Freed, K. F.; Gelbart, W. M. *J. Chem. Phys.* **1972**, *56*, 2309.

(44) Hayashi, M.; Mebel, A. M.; Liang, K. K.; Lin, S. H. *J. Chem. Phys.* **1998**, *108*, 2044.

(45) (a) Werner, H.-J.; Knowles, P. J. *J. Chem. Phys.* **1985**, *82*, 5053. (b) Knowles, P. J.; Werner, H.-J. *Chem. Phys. Lett.* **1985**, *115*, 259.

(46) (a) Becke, A. D. *J. Chem. Phys.* **1993**, *98*, 5648. (b) Lee, C.; Yang, W.; Parr, R. G. *Phys. Rev. B* **1988**, *37*, 785.

(47) (a) Werner, H.-J.; Knowles, P. J. *J. Chem. Phys.* **1988**, *89*, 5803. (b) Knowles, P. J.; Werner, H.-J. *Chem. Phys. Lett.* **1988**, *145*, 514.

(48) Dunning, T. H., Jr. *J. Chem. Phys.* **1989**, *90*, 1007.

(49) (a) Purvis, G. D.; Bartlett, R. J. *J. Chem. Phys.* **1982**, *76*, 1910. (b) Scuseria, G. E.; Janssen, C. L.; Schaefer, H. F., III. *J. Chem. Phys.* **1988**, *89*, 7382. (c) Scuseria, G. E.; Schaefer, H. F., III. *J. Chem. Phys.* **1989**, *90*, 3700. (d) Pople, J. A.; Head-Gordon, M.; Raghavachari, K. *J. Chem. Phys.* **1987**, *87*, 5968.

(50) DALTON, a molecular electronic structure program, Release 1.2, 2001, written by Helgaker, T.; Jensen, H. J. Aa.; Jørgensen, P.; Olsen, J.; Ruud, K.; Ågren, H.; Auer, A. A.; Bak, K. L.; Bakken, V.; Christiansen, O.; Coriani, S.; Dahle, P.; Dalskov, E. K.; Enevoldsen, T.; Fernandez, B.; Hättig, C.; Hald, K.; Halkier, A.; Heiberg, H.; Hettema, H.; Jonsson, D.; Kirpekar, S.; Kobayashi, R.; Koch, H.; Mikkelsen, K. V.; Norman, P.; Packer, M. J.; Pedersen, T. B.; Ruden, T. A.; Sanchez, A.; Saue, T.; Sauer, S. P. A.; Schimmelpfenning, B.; Sylvester-Hvid, K. O.; Taylor, P. R.; Vahtras, O.

(51) MOLPRO is a package of ab initio programs written by Werner, H.-J.; Knowles, P. J., with contributions from Almlöf, J.; Amos, R. D.; Deegan, M. J. O.; Elbert, S. T.; Hampel, C.; Meyer, W.; Peterson, K.; Pitzer, R.; Stone, A. J.; Taylor, P. R.; Lindh, R.

(52) Frisch, M. J.; Trucks, G. W.; Schlegel, H. B.; Scuseria, G. E.; Robb, M. A.; Cheeseman, J. R.; Zakrzewski, V. G.; Montgomery, J. A., Jr.; Stratmann, R. E.; Burant, J. C.; Dapprich, S.; Millam, J. M.; Daniels, A. D.; Kudin, K. N.; Strain, M. C.; Farkas, O.; Tomasi, J.; Barone, V.; Cossi, M.; Cammi, R.; Mennucci, B.; Pomelli, C.; Adamo, C.; Clifford, S.; Ochterski, J.; Petersson, G. A.; Ayala, P. Y.; Cui, Q.; Morokuma, K.; Malick, D. K.; Rabuck, A. D.; Raghavachari, K.; Foresman, J. B.; Cioslowski, J.; Ortiz, J. V.; Stefanov, B. B.; Liu, G.; Liashenko, A.; Piskorz, P.; Komaromi, I.; Gomperts, R.; Martin, R. L.; Fox, D. J.; Keith, T.; Al-Laham, M. A.; Peng, C. Y.; Nanayakkara, A.; Gonzalez, C.; Challacombe, M.; Gill, P. M. W.; Johnson, B.; Chen, W.; Wong, M. W.; Andres, J. L.; Gonzalez, C.; Head-Gordon, M.; Replogle, E. S.; Pople, J. A. *Gaussian 98*, revision A.7; Gaussian, Inc.: Pittsburgh, PA, 1998.

(53) Ibragimova, L. B. *Khim. Fiz.* **1991**, *10*, 307.

(54) (a) Dunn, K.; Morokuma, K. *J. Chem. Phys.* **1995**, *102*, 4904. (b) Cui, Q. Ph.D. Thesis, Emory University, Atlanta, GA, 1998.

(55) NIST Atomic Spectra Data Base, http://physics.nist.gov/cgi-bin/AtData/main_asd.

(56) Peterson, K. A.; Dunning, T. *J. Phys. Chem.* **1995**, *99*, 3898.

(57) Eyring, H.; Lin, S. H.; Lin, S. M. *Basic Chemical Kinetics*; Wiley: New York, 1980.

(58) It should be noted that in the case of the $N_2 + CH$ reaction,[28] the deviation between the theoretical and experimental rate constants was found to be due to the fact that this reaction can occur by another, spin-allowed channel; see: (a) Moskaleva, L. V.; Xia, W. S.; Lin, M. C. *Chem. Phys. Lett.* **2000**, *331*, 269. (b) Moskaleva, L. V.; Lin, M. C. *Proc. Combust. Inst.* **2000**, *28*, 2393.